Journal of Materials Chemistry B

Accepted Manuscript

ROYAL SOCIETY OF CHEMISTRY

www.rsc.org/materialsB

Journal of
Materials Chemistry B

RSCPublishing

ARTICLE

Label-free aptamer biosensor for thrombin detection on nanocomposite of graphene and plasma polymerized allylamine

Cite this: DOI: 10.1039/x0xx00000x

Received 00th January 2012,
Accepted 00th January 2012

DOI: 10.1039/x0xx00000x

www.rsc.org/

Zhihong Zhang[1,2]*, Shunli Liu[1], Yu Shi[1], Yuanchang Zhang[1], Dave Peacock[1], Fufeng Yan[1], Peiyuan Wang[1], Linghao He[1], Xiaozhong Feng[1], and Shaoming Fang[1,2]*

A label-free and effective aptasensor based on amino-functionalized nanocomposite of graphene and plasma-polymerized allylamine (G-PPAA) was developed for thrombin detection. Graphene was assemblied on the substrates, followed by the self-assembly of octadecylamine (OTA) to protect the graphene from etching by subsequent plasma irradiation. Afterward, PPAA was deposited onto the graphene surface with the self-assembled OTA, and the nanocomposite with amino groups was fabricated. The label-free thrombin aptamer was immobilized onto the amino-functionalized nanocomposite matrix through electrostatic interaction between the phosphate groups of aptamer and the amino groups in PPAA. The process was investigated by impedimetric detection and quartz crystal microbalance (QCM). The chemical compositions, surface morphology, and electrochemical properties were found to be dependent on the plasma conditions used in the polymer deposition. The amounts and kinetics of aptamer immobilization and thrombin detection were determined using QCM measurements. Relatively high affinity constant of aptamer immobilization and low detection limit for thrombin were achieved by using the G-PPAA film as the biosensor matrix. Results suggest that G-PPAA films can be applied in gene therapy and protein detection.

1. Introduction

Graphene is a promising material for application in various fields, such as catalysis,[1] energy storage,[2] and electrochemical biosensors,[3] because it has high surface area, excellent conductivity, high chemical stability, and low cost. The applications of graphene are focused on protein adsorption,[4] DNA immobilization,[5,6] and cell adhesion.[7] Graphene is hydrophobic and often forms agglomerates.[8] Functionalization and dispersion of graphene could be improved by using covalent [9] and non-covalent methods.[10] For example, a polyvinylpyrrolidone-modified graphene, which disperses well in aqueous solution, can be used as an electrochemical glucose biosensor.[11] The protein concanavalin A was immobilized onto a self-assembled monolayer of multivalent tripodal molecules on single-layer graphene.[12] In addition, aptamer-conjugated graphene oxide (GO) was used as an affinity extraction and detection platform for analytes from complex biological media.[13] Given the limited amount of biomolecules that can be bonded on a monolayered or modified graphene, various approaches, such as electrochemical,[14] fluorescence,[15] or other spectral techniques,[16] are often applied to evaluate biomolecular adsorption of graphene. However, the adsorption kinetics and amount of biomolecules are difficult to investigate using only these methods.

Aptamers, which are single-stranded oligonucleotides that can naturally fold into different three-dimensional structures, have the capability of binding specifically to a specific target.[17-19] In comparison to antibodies, aptamers can be denatured and refolded multiple times without loss of activity because the aptamer binding function is largely dependent upon simple, stable secondary structural interactions.[20,21] Aptamer-based biosensors, with specificity of biology reactions and high sensitivities of physical transducers, have gained attention in clinical diagnosis. [22,23] The biosensor, which unitilizes the immobilized DNA and RNA aptamers for the selection against several different protein targets, can simultaneously detect and quantify levels of individual proteins in complex biological mixtures.[24]

Reports on the quantitative detection of molecules on graphene-related films have been pubilished. [25-29] Normally,

[1]Henan Provincial Key Laboratory of Surface and Interface Science, [2]Henan Collaborative Innovation Center of Environmental Pollution Control and Ecological Resoration, Zhengzhou University of Light Industry, No. 166, Science Avenue, Zhengzhou 450001, China. E-mail addresses: mainzhh@163.com or mingfang@zzuli.edu.cn fax: + 0086-37186609676 Tel.:+0086-37186609676.

electrochemical, optical or piezoelectric measurements were used to determine the immobilized amounts of aptamer molecules on the sensitive layer. Quartz crystal microbalance (QCM) was used to determine DNA identification on a composite material, which consists of a sheet of graphene-on-Au (111) surface.[30] A surface plasmon resonance (SPR) biosensor based on graphene-on-Au was investigated, and the results showed the high sensitivity of the biosensor.[31]

Plasma-assisted polymerization of monomers containing amino groups, such as allylamine, propylamine, and propargylamine, show interesting properties for biomedical applications.[32] However, allylamine is commonly utilized as organic precursor as well as a matrix of protein and DNA biosensors.[33-26] Quantitative analysis is conducted using the results obtained by SPR because of the high-affinity between the biomolecules and the plasma-polymerized allylamine (PPAA).[37] For example, the mechanical properties of GO is enhanced by its chemical cross-linking with PAH.[38] The conductivity of GO increases after being modified with PAH films.[39] GO-PAH nanofilms could be applied for laser-induced desorption/ionization of small molecules.[40] However, no exact quantitative analysis about the adsorption of biomolecules on the nanocomposite surface of graphene and plasma polymerized films has been conducted. Funtionlized modification of graphene is necessary to improve its bonding interaction with biomolecules as well as its adsorptive capability.

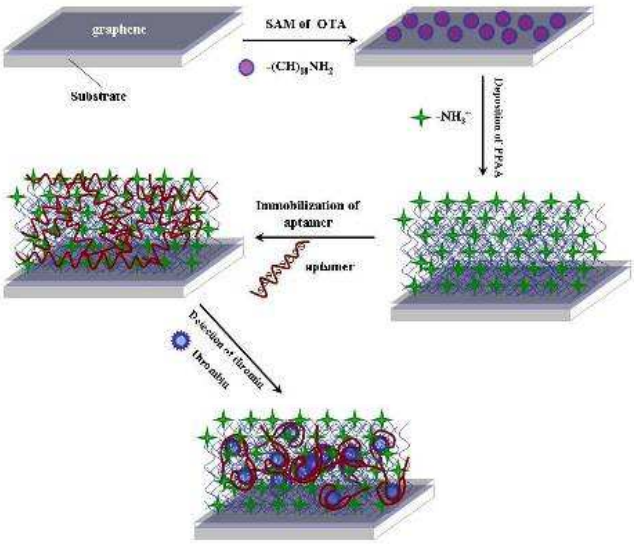

Fig. 1. G-PPAA fabrication, aptamer immobilization on G-PPAA surface through electrostatic interaction strategy, and the mechanism of thrombin detection.

In the present work, G-PPAA films were obtained under various plasma conditions. The chemical structure, surface morphology, and electrochemical properties of the films were investigated. Electrochemical techniques and QCM were applied to evaluate aptamer immobilization and thrombin detection on the surface of the G-PPAA nanofilms. As shown in Scheme 1, octadecylamine (OTA) self-assembled on the graphene surface that was assemblied on Au wafers, followed by the deposition of PPAA under various plasma conditions. Aptamer was subsequently immobilized onto the G-PPAA films because of the electrostatic interaction between the positive charges of $-NH_4^+$ on the PPAA chains and the negative charges of $-PO_4^{3-}$ groups in the aptamer strands in aqueous solution. The fabricated aptasensor was used to detect thrombin molecules.

2. Experimental

2.1 Materials

Graphite powder (325 meshes, 99.95% purity) was obtained from Alfa Aesar. Allylamine was purchased from Aladdin (Shanghai, China). Aptamer (5'-TCTCTCAGTCCGTGGTAGGG CAGGTTG GGGTGACT-3') and thrombin (molecular weight=30,600 Da) were purchased from Shanghai Biotech (China) and used as supplied. Bovine serum albumin (BSA) was obtained from Dingguo Biotech (Beijing, China). IgG and IgE were obtained from Solarbio (Beijing, China). All of the other reagents were analytical grade and used as received. Graphene was prepared by using Hummer's method, [41] followed by dispersion in Milli-Q H_2O.

2.2 Methods

2.2.1 Au slide and silicon wafer modification

Au wafer was used as the working electrode in the electrochemical measurements. And silicon wafer was used in the measurements of AFM and XPS. Quartz chips with Au films for QCM measurements, Au and silicon wafers were cleaned using piranha solution (70% H_2SO_4/30% H_2O_2), followed by washing with Milli-Q H_2O.

2.2.2 Preparation of G-PPAA films by plasma polymerization

For the samples for the measurements of AFM and XPS, graphene was spin-coated directly onto the surface of the silicon substrates. For Au wafer used in the measurements of electrochemical impendence spectroscopy (EIS) and QCM, however, 1-octadecanethiol (ODT) was self-assembled onto the Au surface following by the binding of graphene via the intermolecular interaction. Afterward, to avoid the decomposition of graphene in the plasma reactor and to enhance the compatibility between graphene and the polymeric films, OTA was self-assembled on the graphene surface and then dried using nitrogen gas.

PPAA was deposited onto the graphene with self-assembled OTA under 5, 20 and 100 W plasma input power for various time periods using allylamine as the monomer gas. Plasma polymerization was performed on the HQ-2 PECVD system manufactured by the Institute of Microelectronics of the Chinese Academy of Sciences, China. The radio frequency generator was operated at 13.56 MHz. The gas flow rate was fixed at 10 sccm, and the pressure was kept constant at 0.1 Torr. The other details of the procedures involved are described in the literature.[42] The G-PPAA films on quartz chips coated with Au films for QCM measurements were immersed in phosphate buffer solution (PBS) solution overnight to eliminate unbound monomer molecules or oligomers in the PPAA network.

2.2.3 Preparation of solutions

The aptamer, thrombin, and BSA solutions were prepared using the phosphate buffer solution (PBS) (pH 7.4), which was prepared by mixing 1/15 M Na_2HPO_4 and 1/15 M KH_2PO_4 in $v(Na_2HPO_4):v(KH_2PO_4)$ = (8:2). The electrochemical measurements were performed in the presence of 5 mM $K_3[Fe(CN)_6]$ /$K_4[Fe(CN)_6]$ (1:1) mixture as a redox probe in PBS (pH 7.4, containing 0.1 M KCl). Aptamer was dispersed in PBS at a concentration of 1 μM, then deluted into different concentrations. Thrombin was dispersed in PBS at a concentration of 1000 ng/ mL. BSA solution was prepared by dispersing commercially available BSA in PBS at a concentration of 1 wt.%. All of the solutions were prepared immediately before the experiments and stored at −4 °C until use.

2.2.4 Aptamer immobilization on G-PPAA and thrombin detection

All of the G-PPAA films on quartz chips that were coated with Au films were mounted, and the film equilibration in PBS solution under a dynamic flow was monitored. When the kinetics cuve did not show any clear vatiation, it indicated that the film was stabilized in the solution. Then, the the aptamer solution was circulated into the cell. Time-dependent measurements of aptamer uptake were conducted by measuring the changes in the frequency of QCM chips (ΔF). When no further changes in the frequency were observed, aptamer immobilization was assumed to be complete, and the wet cell was rinsed with PBS to remove the excess aptamer molecules. BSA was subsequently circulated into the flow cell to reduce non-specific adsorption, followed by binding of thrombin. The changes in electrochemical properties of the composite electrode were detected using EIS, whereas the kinetics of the entire procedure was determined by QCM.

2.2.5 Characterization

The surface electronic structure was analyzed by X-ray photoelectron spectroscopy (XPS) using a VG ESCALAB HP photoelectron spectrometer equipped with an analyzer and preparation chambers. An Al Kα ($h\upsilon$ = 1486.6 eV) X-ray source with power ≤100 W was used to record the spectra. The surface morphology was determined using atomic force microscopy (AFM, Nanoscopy IIIa, USA). The samples for Fourier transform infrared (FTIR) spectroscopy were obtained by direct deposition of PPAA on Si wafer spin-coated with graphene. Each FTIR spectrum was collected by cumulating 512 scans at a resolution of 4 cm^{-1}.

2.2.6 Electrochemical measurements

Electrochemical impedance spectroscopy (EIS) was performed using a CHI 660D electrochemical analyzer (Shanghai Chenhua, China). A conventional three-electrode cell was used, which included an Ag/AgCl (saturated KCl) electrode as reference electrode, platinum slides as counter electrode, and Au wafers deposited with PPAA and G-PPAA films as working electrode. The impedance spectra were collected at a potential of −0.2 V_{MSE} in the frequency range of 1 MHz to 1 mHz, with an alternating current amplitude of 5 mV. The spectra were analyzed using Zview2 software, which uses a nonlinear least-squares fit to determine the parameters of the elements in the equivalent circuit.

2.2.7 QCM measurements

AT-cut, 8 MHz quartz piezoelectric crystals (Shanghai Chenhua, China) (1.2 cm diameter, 0.5 mm thickness, and Au-plated on both faces) were used to detect the aptamer immobilization and thrombin detection. The QCM measurement was performed at 9 V (direct current), and the frequency of the vibrating quartz was measured using a Topward high-frequency counter 1220 (Topward Electric Instrument Co., Ltd., Taiwan). The weight on the QCM was calculated using the Sauerbrey equation.[43, 44] Based on the Sauerbrey equation (Eq. 1), the shift of oscillation frequency (ΔF) is proportional to mass change (Δm) on the quartz chip surface when the aptamer is integrated with the QCM system.

$$\Delta F = -[\, 2 f_0^2 / (\mu_q \bullet \rho_q)^{1/2} A \,] \Delta m \qquad (1)$$

where ΔF is the measured decrease in oscillation frequency, f_0 is the frequency of the quartz crystal prior to any mass deposition, which is 8.0×10^6 Hz, Δm is the mass change (g) upon binding, A is the piezoelectricity active area on quartz crystal (0.196 cm^2). Consequently, a 1 Hz change in oscillation frequency is equal to a 1.34 ng change in mass.

3. Results and Discussion

3.1 Chemical components of G-PPAA

The chemical structure of plasma-polymerized films is affected by the plasma conditions, which mainly involve plasma input power, irradiation time, or flow rate of monomer gas, used in film deposition.[45] In the present study, the chemical properties of the G-PPAA film prepared at various plasma input power and duration were investigated and characterized by FTIR and XPS.

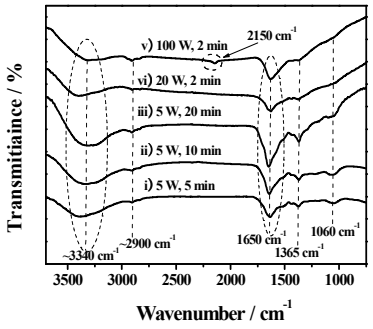

Fig. 2. FT-IR spectra of G-PPAA prepared at 5 W for (i) 5, (ii) 10, and (iii) 20 min and at (iv) 20 and (v) 100 W for 2 min.

Fig. 2 shows the FTIR spectra of the G-PPAA nanocomposites prepared under various plasma conditions. The adsorption band at ~3340 cm^{-1} indicates the presence of primary and secondary amines, and the weak multiple adsorption band at ~2900 cm^{-1} is attributed to CH_x bond stretches. In addition, the broader band around 1650 cm^{-1}

can be assigned to the bending of primary amine groups as well as the stretching of imine groups or C=C groups.[46] XPS characterization was performed to distinguish these groups. The FTIR spectra of G-PPAA also indicate the presence of C-OH (~1365 cm^{-1}) and C-O (~1060 cm^{-1}),[47] which could be attributed to graphene. FTIR spectra were normalized to obtain a semi-quantitative estimation of the relative contents of the functional groups in the G-PPAA films by comparing the relative peak areas. Under the plasma input power of 5 W, the peaks related to primary and secondary amines groups (~3400 cm^{-1}) were unchanged, whereas the peak areas at 1650 cm^{-1} slightly increased along with the weak peak at ~1365 cm^{-1}. The plasma irradiation time showed no significant effect on the chemical structure of the plasma-polymerized nanofilms. However, the areas of the three main peaks declined with increasing plasma input power. The multiple peaks of CH_x at ~2900 cm^{-1} were very weak in all of the cases. This phenomenon is different from that of the pure PPAA films, which includes apparent CH_x groups under both low and high plasma input power. Similar results were also found in the XPS spectra of C1s (Table 1), which were definitely related to the addition of graphene in plasma-polymerized films.

Table 1 Atomic % of G-PPAA prepared under various plasma conditions.

Sample	C (%)	N (%)	O (%)
5 W, 5 min	58.82	16.2	24.99
5 W, 10 min	55.28	18.52	26.2
5 W, 20 min	55.48	18.8	25.72
20 W, 2 min	54.12	16.42	29.46
100 W, 2 min	53.22	13.61	33.17

The chemical compositions of the G-PPAA films deposited at 5 W for various time periods, as well as at 20 and 100 W for 2 min, are summarized in Table 1. All of the nanofilms were rich in nitrogen. Oxygen was also observed in the G-PPAA nanocomposites, which was due to the following reasons: (i) oxygen contamination during plasma irradiation[48] and (ii) the presence of oxygen in the pristine graphene.[49] Under the same plasma input power (5 W), the concentration of carbon in the G-PPAA film produced by the 10 min deposition was less than that in the G-PPAA produced by the 5 min deposition. After extending the plasma deposition time to 20 min, the carbon content was maintained at approximately 55.28% to 55.48%. Meanwhile, the concentration of nitrogen in the G-PPAA film increased from 16.2% to 18.52% when the duration of plasma deposition was increased from 5 min to 10 min. No substantial variation in the nitrogen concentration of G-PPAA deposited for 20 min was observed thereafter. Moreover, the concentration of oxygen remained constant (~25%). As the input power changed from 5 W to 100 W, the concentrations of carbon and nitrogen in the G-PPAA films decreased, whereas that of oxygen substantially increased. This observation is mainly due to the decomposition of G-PPAA under high plasma input power, wherein more carbon and nitrogen atoms were irradiated and reacted with oxygen species to form gas molecules that were subsequently removed from the surface of the films.

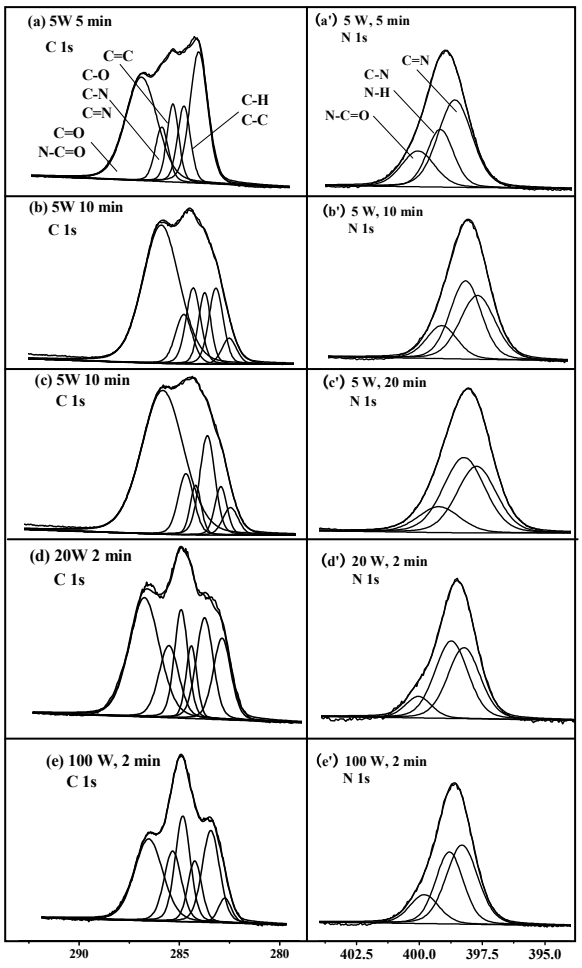

Fig. 3. C1s and N1s core-level XPS spectra and their corresponding peaks in the G-PPA films deposited at 5 W (5, 10, and 20 min), 20 W (2 min), and 100 W (2 min).

To analyze the variations in the functional groups found in the G-PPAA films, the peak-fitted C1s and N1s core-level XPS spectra are summarized in Fig. 3. In the C1s spectra of all of the G-PPAA nanofilms, the same fits mainly contain four component peaks, which correspond to the different chemical environments present in the sample. The peak at ~284.6 eV is assigned to CH_x, which was very weak in the FTIR spectra. The peak at ~285.2 eV is due to C=C, whereas the peak at ~285.7 eV is possibly due to C-N (primary, secondary, or tertiary amine groups), C=N (imine), and C-O (alcohol or ether). The peak at 287 eV is possibly due to C=O (carbonyl) and N-C=O (amide). A peak at ~283.8 eV was observed in the sample deposited at 5 W for 5 min. This peak separated into two parts (~284 and 283.3 eV) when the G-PPAA films were prepared for a long time at 5 W or at high input power. However, this peak, which should be assigned to the groups of $–(C^*H_2\text{-}CH_2)_n$

on the plasma polymer (Holm), was not found in the C1s of the pristine graphene and PPAA films.[50, 51] The N1s core-level XPS spectra of the samples mainly consist of three components, which can be deconvoluted into C=N (~399.3 eV), C-N/N-H (~399.8 eV), and N-C=O (~401.3 eV).

The contents of the functional carbon-related and nitrogen-related groups in the G-PPAA surface were determined by their relative density in C1s and N1s, as well as in the atomic percent of C and N (Fig. 4). The C=C group content in the G-PPAA decreased from 7.1% to 3.0% in various durations of plasma deposition at 5 W. However, the C=C group content increased up to 10.1% when high plasma input power was employed. Under plasma, the C=C bonds in allylamine could be irradiated and broken, leading to the formation of sp^3 CH_3 or sp^3 CH_2 groups in the polymeric structure.[52] C=C bonds could also be produced when the hydrogen is lost through the transformation of sp^3 CH_3 or sp^3 CH_2 groups on polymer chains into sp^2 configuration.[53] These contradicting directions coexist in the plasma system, and they are dependent on the plasma conditions used. At low input power (5 W), □ bonds in the C=C groups of allylamine are opened by the free radicals produced by the irradiation of plasma, leading to the deposition of polymeric films.[54] As the plasma deposition continues, more allylamine molecules are polymerized into the polymeric structure with low C=C group density. By contrast, under high input power, the breakage of sp^3 carbon groups dominates the system, indicating that more sp^2 carbon groups are in the polymer chains.[55] Compared with the C=N/N-C=O groups in the C1s core-level spectra whose content ranges from 25% to 33% in the G-PPAA films deposited at 5 W, 18.7% at 20 W, and 8.2 % at 100 W [Fig. 4 (a)], the N-C=O group content in the N1s core-level spectra is less than 3.1%. The difference is attributed to the large amounts of C=O that originate from graphene or the oxidation of the PPAA films. Meanwhile, the difference between the C=N/C-N/C-O content in the C1s spectra and that of C=N/C-N/N-H in the N1s spectra was due to the high amino group content.

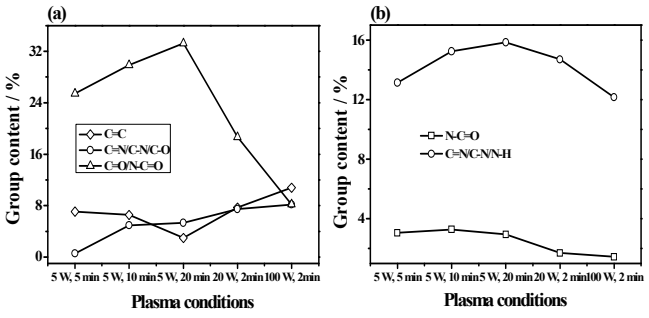

Fig. 4. Relative intensity of functional (a) carbon-related and (b) nitrogen-related groups of G-PPAA deposited at 5 W (5, 10, and 20 min), 20 W (2 min), and 100 W (2 min).

3.2 Surface morphology of G-PPAA

AFM images were obtained to investigate the effect of plasma input power on the surface morphology of the deposited G-PPAA (Fig. 5). The pristine graphene showed a smooth surface with an average roughness (R_a) of 0.33 nm (Fig. 5 (a)). After the deposition of PPAA on the graphene surface at 5 W for 5 min, the R_a of the material increased to 0.39 nm (Fig. 5 (b)); some nanoparticles formed during plasma irradiation. The surface morphologies of G-PPAA prepared at 20 W for 2 min (Fig. 5 (c)) and at 100 W for 2 min (Fig. 5 (d)) are very similar with that of G-PPAA deposited at 5 W. This observation clearly indicates that a homogenous G-PPAA surface can be achieved at the optimal plasma condition. In this case, the effect of the surface morphology of G-PPAA on the adsorption of biomolecules could be neglected.

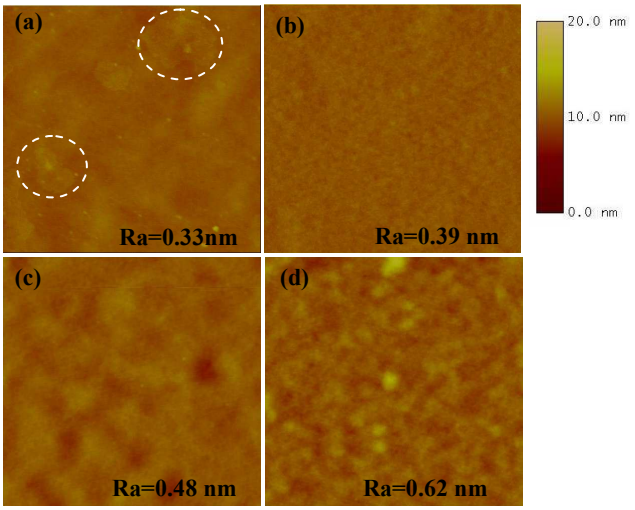

Fig. 5 Two-dimensional AFM images of (a) the pristine graphene and G-PPAA films deposited at (b) 5 W for 5min, (c) 20 W for 2 min, and (c) 100 W for 2 min.

3.3 Electrochemical properties of G-PPAA before and after aptamer immobilization and thrombin detection

EIS is an effective tool for monitoring the changes in the surface features of modified electrodes in the assembly process; EIS has been used to determine the adhesion of biomolecules, bacteria, or cells. The impedance spectra include a semicircle portion and a linear portion. The semicircle portion at high frequencies corresponds to the electron transfer process, whereas the linear portion at lower frequencies represents the diffusion process. The semicircle diameter is equal to the electron-transfer resistance, R_{et}.[56] Fig. 6 shows the EIS of the PPAA and G-PPAA films deposited under 5, 20, and 100 W. The simulated value of R_{et} of PPAA are 34.51, 76.23, and 94.86 KΩ. And R_{et} of G-PPAA are 29.75, 53.24, and 71.32KΩ. The results show that the R_{et} increases with the plasma input power used in the preparation of PPAA and G-PPAA films increasing, indicating that the high electrochemical activity of the films deposited at the low plasma input power. Additionally, the smaller R_{et} value of G-PPAA films hints its higher electrochemical activities due to the good electrochemical properties of the pristine graphene. [57]

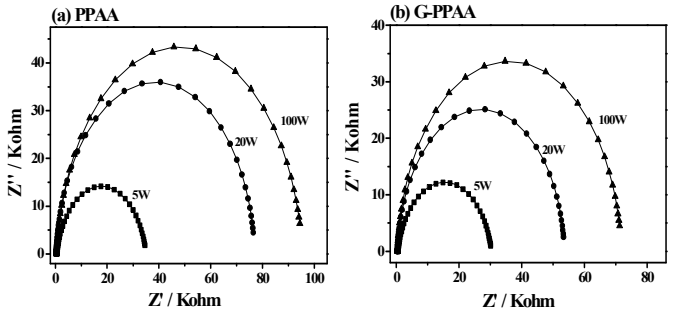

Fig. 6 Nyquist disgrams of EIS of (a) PPAA and (b) G-PPAA films deposited under 5, 20, and 100 W.

Fig. 7 shows the EIS of the electrode at various stages.The simulated values of R_{et} for the different stages are also summarized in Table 2. For the Au electrode, which was self-assembled with ODT, the R_{et} value was 2.68 KΩ. When graphene was self-assembled on ODT (Au-ODT-G), a much lower resistance of 1.13 KΩ was found. This observation indicates that the presence of graphene could improve the electrical conductivity of the electrode. R_{et} of the composite electrode increased to 4.18 KΩ after the self-assembly of OTA on the surface of the graphene. This phenomenon may be due to the generation of a surface with decreased conductivity on the self-assembled layer, which inhibited the access of the electrons to the modified surface. The value of R_{et} continuously increased to 29.75 KΩ after the deposition of PPAA on the graphene surface. This observation may be caused by the PPAA film insulation, leading to the slow transfer of electrons at the interface between the G-PPAA and the electrolyte solution.[58]

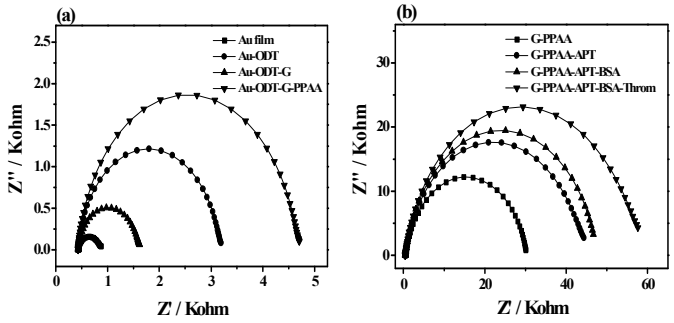

Fig. 7 Nyquist disgrams of EIS for (a) each stage of G-PPAA films deposited at 5 W on Au wafer self-assembled with ODT and (b) the immobilization of aptamer and the detection of thrombin on the surface of G-PPAA film.

In aqueous solutions, the aptamer could be immobilized onto G-PPAA surface because of the strong electrostatic interaction between the positive charges of the amino groups in the PPAA molecule chains and the negative charges of the phosphate groups in the aptamer strands. Given that no special conformation in the aptamer molecules was observed before bonding with proteins, the aptamer strands only covered the surface of the G-PPAA, thereby inhibiting the electron transfer and increasing the R_{et} value from 29.75 KΩ to 41.84 KΩ. To eliminate the non-specific adsorption between thrombin and the G-PPAA surface, BSA was used for pre-adsorption, which also increased R_{et} (5.23 KΩ). Aptamers exhibiting binding affinities to thrombin, and the folding motifs of the aptamers and their three-dimensional structures that bind to thrombin were elucidated by spectroscopic and NMR methods.[59] When an aptamer molecule is bonded with thrombin, the R_{et} value increased from 47.07 KΩ to 54.51 KΩ. This is attributed to the fact that an insulating layer on the surface and the transfer of redox couple $[Fe(CN)_6]^{3-/4-}$ to the surface of Au film is prohibited.

Table 2 R_{et} values of the composite electrodes at various stages during aptamer immobilization and thrombin detection.

Stage	R_{et} (KΩ)	ΔR_{et} (KΩ)
Au film	0.38	
Au-ODT	2.68	2.30
Au-ODT-G	1.13	-1.55
Au-ODT-G-OTA	4.18	3.05
Au-ODT-G-OTA-PPAA	29.75	25.57
Au-ODT-G-OTA-PPAA-Apt	41.84	11.09
Au-ODT-G-OTA-PPAA-Apt-BSA	47.07	5.23
Au-ODT-G-OTA-PPAA-Apt-BSA-Throm	54.51	7.44

3.4 Amount of immobilized aptamer on G-PPAA films

Film thickness, which is dependent on the deposition rate, is important in the adsorption of biomolecules on the surface of plasma polymers.[60] Film thickness typically increases with increasing plasma irradiation time.[61] The relationship between the adsorbed amount of aptamer molecules and the thickness of G-PPAA films was evaluated. QCM measurement was performed to determine the adsorbed amount of aptamer on the G-PPAA films deposited at 5 W for various time periods (Fig. 8). The observed thickness values of the G-PPAA films under 5 W plasma depositions were 21, 45, and 69 nm for 5, 10, and 20 min, respectively. Studies on QCM-based biomolecular interaction were not performed on nanocomposite films prepared by plasma polymerization. QCM is a sensitive mass sensor, in which an increase in mass on the quartz surface causes a decrease in the oscillation frequency of the crystal.[62]

Fig. 8 demonstrates the binding of aptamer molecules with the PPAA and G-PPAA films deposited at 5 W for different periods of time, 5, 10, and 20 min. For all of the samples, aptamer adhesion reached equilibrium within 30 min after the aptamer was circulated into the flow cell. The systems were allowed to stabilize over periods of 15 min to 20 min, and no further significant changes were observed. After the stabilization stage, pure PBS was incubated into the system, which always led to a loss of some unbound aptamers from the surface. After a few minutes, the aptamer adhesion level reached a new equilibrium. Herein, Δm values were calculated from ΔF by according to the equation (1). The Δm values of the aptamer molecules immobilized onto the PPAA films deposited at 5 W for 5, 10, and 20 min were 416.58,

535.67, and 790.04 ng, respectively. Additionally, the Δ*m* values of the aptamer molecules immobilized onto the G-PPAA films deposited at 5 W for 5, 10, and 20 min were 448.07, 677.17, and 891.14 ng, respectively. It demonstrates the aptamer showed preference to adsorbing onto the thick films which was deposited at a long period of time. It mainly could be due to the larger space of the network and relatively high amount of amino groups on the thick films.[37] Moreover, the amount of aptamer molecules immobilized on G-PPAA films are higher than that on PPAA films prepared at the same plasma condition. It clear shows that the presence of graphene could not only enhance the electrochemical activity of the plasma films but also improve the sensitivity of aptamer sensing.

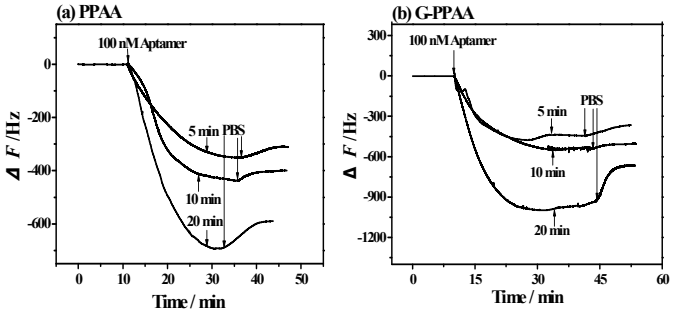

Fig. 8 Kinetic curves of the immobilization of aptamer on (a) PPAA and (b) G-PPAA films deposited at 5 W for 5, 10, and 20 min.

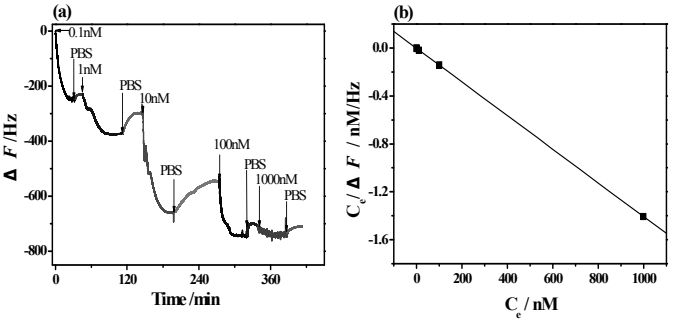

Fig. 9 (a) Frequency response profiles for the immobilization of the aptamer at different concentrations of 0.1, 1, 10, 100, and 1000 nM. (b) Linear calibration curve for the $C_e/\Delta F$ versus C_e, where C_e is the concentration of the aptamer.

3.5 Efficiency of aptamer immobilization on the G-PPAA films

The G-PPAA film deposited at 5 W for 20 min was used as the matrix for thrombin aptasensors. As shown in Fig. 9(a), the G-PPAA-modified quartz chip was incubated with aptamer at various concentrations from 0.1 nM to 1000 nM to evaluate the efficiency of the aptasensor. Using a stepwise increase in the aptamer concentration, new equilibrium states associated with a particular oscillation frequency were reached. The oscillation frequency observed after equilibration of each step allows for a quantitative evaluation of the affinity constant (K_A). If the oscillation frequency is plotted as a function of the aptamer concentration, or as the linear version of the Langmuir isotherm, $C_e/\Delta F$ versus C_e, then the affinity constant K_A can be calculated [Fig. 9(b)]. The obtained equation was $C_e/\Delta F = (-0.00208) + (-0.0014)\ C_e$ with a regression coefficient of 0.99932. Thus, K_a was 0.69 nM^{-1}, and the saturated adsorbed amount of aptamer was 956.76 ng.

3.6 Optimization of thrombin detection

After the aptamer immobilization on the G-PPAA films, non-specific adsorption was eliminated by BSA adsorption. Thrombin of different concentrations was subsequently incubated into the flow cell of the QCM. As for G-PPAA film, a linear relationship between ΔF and the logarithmic values of thrombin concentrations was calculated to be in the range of 5 ng/mL to 1000 ng/mL (See Fig. 10), $\Delta F = 545.092 - 731.083$ lg (C_{thrombin}/ng/mL), with a correlation coefficient of 0.99044 (n=6). The limit of detection was estimated to be 5.57 ng/mL, i.e., 0.182 nM, which were close to that for the other thrombin-aptasensor by QCM.[63, 64]

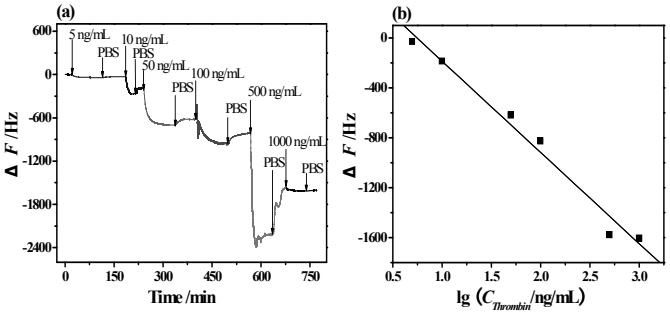

Fig. 10 (a) Frequency response profiles for the detection of thrombin at different concentrations of 5, 10, 50, 100, 500, and 1000 ng/mL. (b) Linear calibration curve for ΔF versus lg ($C_{thrombin}$/ng/mL), where $C_{thrombin}$ is the concentration of thrombin.

3.7 The selectivity of the aptamer-based biosensor

To determine the selectivity of the aptamer-based biosensor, the other proteins (IgG and IgE) at the concentration of 100 ng/mL was tested under the same conditions as in the case of thrombin, compared with thrombin detection at a concentration of 10 ng/mL (Fig. 12). It was easily observed that all other proteins produce weak signal on the QCM crystals, though they have the concentration 10 times more than thrombin. The reason is that only thrombin can combine with specific aptamer sequence.

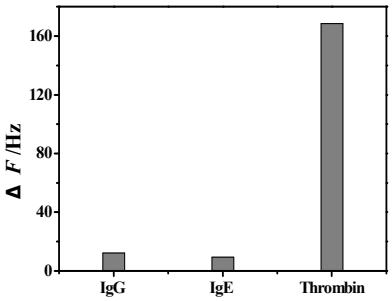

Fig. 11 ΔF of the detection of 10 ng/mL thrombin, 100 ng/mL IgG, and 100 ng/mL IgE.

4. Conclusions

A new aptamer sensor for thrombin detection was developed on an amino-functionalized nanocomposite film fabricated on graphene surface by plasma polymerization and self-assembly. The chemical compositions of the G-PPAA films were dependent on the plasma conditions, in which the plasma input power has a more important role. The presence of graphene could not only enhance the electrochemical activity of the plasma films but also improve the sensitivity of aptamer sensing. In addition, the electrochemical properties of the G-PPAA films decreased because of the difficulties in electron transfer along the interface of the electrolyte and the composite electrode, which is due to aptamer immobilization. After the bonding of thrombin on the aptamer, the electrochemical activity increased because of the conformation change in the aptamer and the improved transfer channel of electrons. A high affinity constant K_a of aptamer bonding on the G-PPAA film was obtained, with the highest saturated adsorbed aptamer amount of 956.76 ng. Moreover, the limit of thrombin detection was approximately 5.57 nM, which is close to that of the other system. Easy preparation, high functionalization, quantitative biomolecule bonding, and good biocompatibility suggest that G-PPAA can be applied in gene therapy and protein detection.

Acknowledgements

This work was supported by Program for the National Natural Science Foundation of China (NSFC: Account No. 51173172 and 21104070).

Notes and references

1 J. D. Roy-Mayhew, D. J. Bozym, C. Punckt and I. A. Aksay, *ACS Nano*, 2010, **4**, 6203-6211.

2 H. Gwon, H. S. Kim, K. U. Lee, D. H. Seo, Y. C. Park, Y. S. Lee, B. T. Ahn and K.Kang, *Energy Environ. Sci*., 2011, **4**, 1277-1283.

3 J. Zhao, G. Chen, L. Zhu and G. Li, *Electrochem. Commun*., 2011, **13**, 31-33.

4 Y. Ohno, K. Maehashi, Y. Yamashiro and K. Matsumoto, *Nano Lett.*, 2009, **9**, 3318-3822.

5 B. Gulbakan, E. Yasun, M. I. Shukoor, Z. Zhu, M. You, X. Tan, H. Sanchez, D. H. Powell, H. Dai and W. Tan, *J. Am. Chem. Soc.*, 2010, **132**, 17408-17410.

6 M. Du, T. Yang and K. Jiao, *J. Mater. Chem.*, 2010, **20**, 9253-9260.

7 C. X. Guo, X. T. Zheng, Z. S. Lu, X. W. Lou and C. M. Li, *Advanced Materials*, 2010, **22**, 5164-5167.

8 D. Li, M. B. Müller, S. Gilje, R. B. Kaner and G. G. Wallace. *Nature Nanotechnology*, 2008, **3**, 101-105.

9 Y. Xu, Z. Liu, X. Zhang, Y. Wang, J. Tian, Y. Huang, Y. Ma, X. Zhang and Y. Chen, 2009, **21**, 1275-1279.

10 H. Bai, Y. Xu, L. Zhao, C. Li and G. Shi, *Chem. Commun.*, 2009, 1667-1669.

11 C. Shan, H. Yang, J. Song, D. Han, A. Ivaska and L. Niu, *Anal. Chem.*, 2009, **81**, 2378-2382.

12 T. Alava, J. A. Mann, C. Theodore, J. J. Benitez, W. R. Dichtel, J. M. Parpia and C H. G. raighead, *Anal. Chem.* 2013, **85**, 2754-2759.

13 B. Gulbakan, E. Yasun, M. I. Shukoor, Z. Zhu, M. You, X. Tan, H. Sanchez, D. H. Powell, H. Dai and W. Tan, *J. Am. Chem. Soc.*, 2010, **132**, 17408-17410.

14 S. Alwarappan, A. Erdem, C. Liu and C. Li, *J. Phys. Chem. C*, 2009, **113**, 8853-8857.

15 H. Dong, W. Gao, F. Yan, H. Ji and H. Ju, *Anal. Chem.*, 2010, **82**, 5511-5517.

16 Z. Tang, H. Wu, J. R. Cort, G. W. Buchko, Y. Zhang, Y. Shao, I. A. Aksay, J. Liu and Y. Lin, *Small*, 2010, **6**, 1205-1209.

17 C. Pestourie, B. Tavitian and F. Duconge, *Biochimie*, 2005, **87**, 921–930.

18 C. A. Savran, S. M. Knudsen, A. D. Ellington and S. R. Manalis, *Anal Chem*, 2004, **76**, 3194–3198.

19 R. Stoltenburg, C. Reinemann and B. Strehlitz, *Biomol Eng*, 2007, **24**, 381–403

20 R. Kirby, E. J. Cho, B. Gehrke, T. Bayer, Y. S. Park and D. P. Neikirk, *Anal Chem*, 2004, **76**, 4066–4075.

21 M. Liss, B. Petersen, H. Wolf and E. Prohaska, *Anal Chem*, 2002, **74**, 4488–4495.

22 A. Buhl, J. H. Metzger, N. H. H. Heegaard, P. Landenberg, M. Fleck and P. B. Luppa, *Clin Chem*, 2007, **53**, 334–341.

23 B. F. Yuan, Y. H. Hao and Z. Tan, *Clin Chem*, 2004, **50**, 1057–1060.

24 T. G. Mccauley, N. Hamaguchi and M. Stanton, *Anal Biochem*, 2003, **319**, 244–250.

25 Z. Zhang, L. Luo, L. Zhu, Y. Ding, D. Deng and Z. Wang, *Analyst*, 2013,**138**, 5365-5370.

26 Y. Wang, Y. Xiao, X. Ma, N. Lia and X. Yang, *Chem Commun*, 2012, **48**, 738-740.

27 J. Liu, L. Tao, W. Yang, D. Li, C. Boyer, R. Wuhrer, F. Braet and T. P. Davis, *Langmuir*, 2010, **26**, 10068–10075.

28 Y. Yao, X. Chen, H. Guo and Z. Wu, *Applied Surface Science*, 2011, **257**, 7778-7782.

29 Y. Yao, X. Chen, X. Li, X. Chen and N. Li, *Sensor Actuat B*, 2014, **191**, 779-783.

30 J. Cai, P. Ruffieux, R. Jaafar, M. Bieri, T. Braun, S. Blankenburg, M. Muoth, A. P. Seitsonen, M. Saleh, X. Feng, K. Müllen and R. Fasel, *Nature*, 2010, **466**, 470-473.

31 M. Islam, A. Z. Kouzani, X. J. Dai, W. P. Michalski and H. Gholamhosseini, J. *Biomed. Nanotechnol*., 2012, **8**, 380-393.

32 K. Vasilev, L. Britcher, A. Casanal and H. J. Griesser, *J. Phys. Chem. B*, 2008, **112**, 10915-10921.

33 M. A. Dyer, K. M. Ainslie and M. V. Pishko, *Langmuir*, 2007, **23**, 7018-7023.

34 M. R. Kreke, A. S. Badami, J. B. Brady, R. M. Akers and A. S. Austein, *Biomaterials*, 2005, **26**, 2975-2981.

35 Q. Chen, R. Förch and W. Knoll, *Chem. Mater.*, 2004, **16**, 614-620.

36 J.J.J.P. Van den Beucken, M.R.J. Vos, P.C. Thüne, T. Hayakawa, T. Fukushima, Y. Okahata, X.F. Walboomers, N.A.J.M. Sommerdijk, R.J.M. Nolte and J.A. Jansen, *Biomaterials*, 2006, **27**, 691-701.

37 Z. Zhang, Q. Chen, W. Knoll, R. Foerch, R. Holcomb and D. Roitman, *Macromolecules*, 2003, **36**, 7689-7694.

38 A. Satti, P. Larpent and Y. Gun'ko, *Carbon*, 2010, **48**, 3376-3381.

39 B. S. Kong, H. W. Yoo and H. T. Jung, *Langmuir*, 2009, **25**, 11008-11013.

40 Y. K. Kim and D.Min, *Langmuir*, 2012, **28**, 4453-4458.

41 H. Guo, X. Wang, Q. Qian, F. Wang and X. Xia, *ACS Nano.*, 2009, **3**, 2653-2659.

42 Z. Zhang, J. Dou, F. Yan, X. Zheng, X. Li and S. M. Fang, *Plasma Processes Polym.*, 2011, **8**, 923-931.

43 X. Su and Y. Li, *Biosens and Bioelectron,* 2005, **21**, 840-848.

44 J. Kankare, *Langmuir*, 2002, **18**, 7092-7094.

45 D. Hegemann and M. Hossain, *Plasma Processes Polym*, 2005, **2**, 554-562.

46 C. Hontoria-Lucas, A. J. López-Peinado, J. D. López-González, M.L. Rojas-Cervantes and R. M. Martín-Aranda, *Carbon*, 1995, **33**, 1585-1592.

47 R. Hao, W. Qian, L. Zhang and Y. Hou, *Chem. Commun*, 2008, 6576-6578.

48 Z. Zhang, P. Liang, X. Zheng, D. Peng, F. Yan, R. Zhao and C. L. Feng , *Biomacromolecules*, 2008, **9**, 1613-1617.

49 Z. Sun, Z. Yan, J. Yao, E. Beitler, Y. Zhu and J. M. Tour, *Nature*, 2010, **468**, 549-552.

50 X. Li, G. Zhang, X. Bai, X. Sun, X. Wang, E. Wang and H. Dai, *Nature Nanotechnology* ,2008, **3**, 538-542.

51 M. Tatoulian, F. Brétagnol, F. Arefi-Khonsari, J. Amouroux, O. Bouloussa, F. Rondelez, A. J. Paul and R. Mitchell, *Plasma Process Polym*, 2005. **2** , 38-44.

52 D. J. Menzies, B. Cowie, C. Fong, J. S. Forsythe, T. R. Gengenbach, K. M. McLean, L. Puskar, M. Textor, L. Thomsen, M. Tobin and B. W. Muir, *Langmuir*, 2010, **26**, 13987-13994.

53 J. Ristein, R. T. Stief, L. Ley and W. Beyer, *J Appl Phys.* ,1998, **84**, 3836-3847.

54 Z. F. Li, A. N. Netravali and W. Sachse, *J Appl Polym Sci.*, 1992, **27**, 4625-4632.

55 P. Couderc and Y. Catherine, *Thin Solid Films*, 1987, **146**, 93-107.

56 G. Zhao, J. J. Xu and H. Y. Chen, *Electrochem Commun*, 2006, **8**, 148-154.

57 W. Yang, X. Zhu, Q. Liu, Z. Lin, B. Qiu and G. Chen, *Chem Commun*, 2011, **47**, 3129-3131.

58 M. Tatoulian, F. Brétagnol, F. Arefi-Khonsari, J. Amouroux, O. Bouloussa, F. Rondelez, A. J. Paul and R. Mitchell. *Plasma Process Polym*, 2005, **2**, 38-44.

59 J. A. Kelly, J. Feigon and T. O. Yeates, *J Mol Biol,* 1996, **256**, 417-422.

60 W. Yang, S. Chen, G. Cheng, H. Vaisocherová, H. Xue, W. Li, J. Zhang and S. Jiang, *Langmuir*, 2008, **24**, 9211-9214.

61 H. Yasuda, *Plasma Polymerization*, Academic Press Inc.: Orlando, FL, 1985.

62 D. A. Buttry and D. M. Ward, *Science*, 1990, **249**, 1000-1007.

63 A. Porfirieva, G. Evtugyn and T. Hianik, *Electroanalysis*, 2007, **19**, 1915-1920.

64 T. Hianik, V. Ostatná, Z. Zajacová, E. Stoikova and G. Evtugyn, *Bioorg. Med. Chem. Lett.*, 2005, **15**, 291-295.